PERGAMON

International Journal of Heat and Mass Transfer 43 (2000) 2257–2266

International Journal of HEAT and MASS TRANSFER

www.elsevier.com/locate/ijhmt

Natural convection from a discrete heat source on the bottom of a horizontal enclosure

I. Sezai*, A.A. Mohamad

Department of Mechanical Engineering, Eastern Mediterranean University, G. Magosa, Mersin 10, Turkey

Received 9 June 1999; received in revised form 7 October 1999

Abstract

Steady, natural convection from a discrete flush-mounted rectangular heat source on the bottom of a horizontal enclosure is studied numerically. Three-dimensional form of Navier–Stokes equations are solved by using multigrid technique. Rayleigh number based on the enclosure height is varied from 10^3 until unstable flow is predicted for a fixed Prandtl number of 0.71. Aspect ratio of the source is varied until it fully covered the entire width of the bottom plate. The enclosure is cooled from above and insulated from the bottom. Effect of vertical boundary conditions on the rate of heat transfer from the heat source is studied. It is found that the rate of heat transfer is not so sensitive to the vertical wall boundary conditions. The limit of the maximum Rayleigh number to obtain a convergent solution decreases as the aspect ratio of the source is increased. The variation of Nusselt number as a function of Rayleigh number and aspect ratio of the source is reported.

Keywords: Numerical simulation; Discrete heat source; Natural convection; Horizontal enclosure; Multigrid method

1. Introduction

Natural convection has been considered an effective way of cooling electronic equipment due to its high reliability, low maintenance cost, and absence of noise. Considerable attention has been given to natural convection from vertical enclosures with discrete heat sources attached on the vertical wall [1–6]. The problem of discrete heat source attached on a horizontal surface of an electronic package is of equal importance. However, there are very few contributions to the buoyancy induced flow over a discrete heat source mounted on a horizontal wall of an enclosure. Polentini et al. [7] reported that a horizontal alignment of discrete heat sources is preferred when uniform heat transfer rates are desired from different rows, which is most often the case for electronic cooling.

The natural convection from a discrete flush-mounted rectangular heat source on the bottom of a horizontal enclosure has a direct resemblance to Raleigh–Bénard problem, which consists of an enclosure heated from below and cooled from top. The induced flow pattern consists of rotating rolls or mushroom type structure depending on *Ra*, *Pr*, and geometrical constraints. This problem has been studied extensively and recent reviews can be found in Refs. [8] and [9]. For a cubic cavity, the critical Rayleigh number for the onset of convection in the Raleigh–Bénard problem is 3446 and 7000 for adiabatic and conducting lateral walls, respectively. Supercritical range for Ray-

* Corresponding author. Fax: +90-392-366-1217.
E-mail address: sezai@menet.me.emu.edu.tr (I. Sezai).

0017-9310/00/$ - see front matter
PII: S0017-9310(99)00304-X

Nomenclature

A_x	aspect ratio of enclosure in x-direction, L_x/H
A_y	aspect ratio of enclosure in y-direction, L_y/H
a_x	aspect ratio of discrete heater in x-direction, l_x/H
a_y	aspect ratio of discrete heater in y-direction, l_y/H
H	height of enclosure
k	thermal conductivity
L_x, L_y	enclosure dimensions in x-, y- directions, respectively
l_x, l_y	dimensions of the discrete heater in x- and y- directions, respectively
Nu	local Nusselt number, hH/k
P	nondimensional pressure, $p/\rho u_r^2$
p	pressure
Pr	Prandtl number, ν/α
Ra	Rayleigh number, $g\beta(t_h - t_c)H^3/\nu\alpha$
T	non-dimensional temperature, $(t - t_c)/(t_h - t_c)$
t	temperature
U, V, W	non-dimensional Cartesian velocities u/u_r, v/u_r, w/u_r, respectively
u, v, w	Cartesian velocities
u_r	reference velocity, ν/H
X, Y, Z	non-dimensional Cartesian coordinates, x/H, y/H, z/H respectively
x, y, z	Cartesian coordinates
α	thermal diffusivity
ϕ	U, V, W, P, or T field
ν	kinematic viscosity
ρ	density

Subscripts

c	cold
h	hot

leigh number is 4000–8000 for adiabatic lateral walls. The critical Rayleigh number decreases as the aspect ratio of the cavity increases.

The object of this study is to examine the heat transfer and natural convection due to a discrete heat source, mounted flush with the bottom wall of a rectangular enclosure. The resulting flow structure is analyzed to provide a fundamental understanding of the effect of Rayleigh number and the lateral aspect ratio of the discrete heat source on the velocity and thermal fields with the aid of the information gained from Raleigh-Bénard problem. The lateral dimension of the source is varied until it covers the entire width of the bottom plate.

2. Physical model

Fig. 1 shows the schematic diagram of the problem under consideration, which consists of a chip of constant surface temperature in an enclosure having width L_x, depth L_y, and height H. The aspect ratios $A_x = L_x/H$ and $A_y = L_y/H$ of the enclosure are set to be equal to 4. The chip is flush-mounted with the bottom horizontal wall and has dimensions l_x and l_y in x- and y-directions respectively. The longitudinal aspect ratio $a_x = l_x/H$ of the chip is set to be unity while the lateral aspect ratio $a_y = l_y/H$ is varied between 1 and 4. The bottom wall surface is assumed to be adiabatic, except the chip, while the upper wall surface is maintained at temperature t_c. For the sidewalls of the enclosure two kinds of boundary conditions are considered: (1) adiabatic and (2) constant temperature sidewalls at t_c.

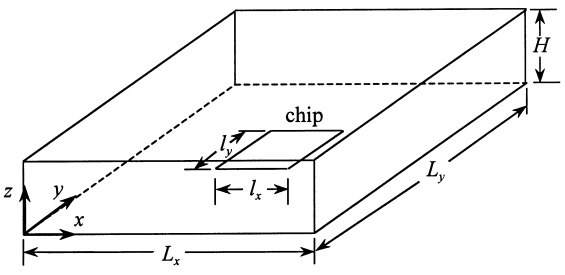

Fig. 1. Schematic diagram of physical configuration and the coordinate system.

3. Governing equations

A three-dimensional (3D), steady state, incompressible laminar flow model is considered in the present study. All properties are assumed to be constant except that the effect of density variations on buoyancy is retained, by using the Boussinesq approximation. The dimensionless governing equations based on the above assumptions are as follows.

Continuity

$$\frac{\partial U}{\partial X} + \frac{\partial V}{\partial Y} + \frac{\partial W}{\partial Z} = 0 \tag{1}$$

x-Momentum,

$$U\frac{\partial U}{\partial X}+V\frac{\partial U}{\partial Y}+W\frac{\partial U}{\partial Z}=-\frac{\partial P}{\partial X}+\nabla^2 U \tag{2}$$

y-Momentum,

$$U\frac{\partial V}{\partial X}+V\frac{\partial V}{\partial Y}+W\frac{\partial V}{\partial Z}=-\frac{\partial P}{\partial Y}+\nabla^2 V \tag{3}$$

z-Momentum,

$$U\frac{\partial W}{\partial X}+V\frac{\partial W}{\partial Y}+W\frac{\partial W}{\partial Z}=-\frac{\partial P}{\partial Z}+\nabla^2 W+\frac{RaT}{Pr} \tag{4}$$

Energy,

$$U\frac{\partial T}{\partial X}+V\frac{\partial T}{\partial Y}+W\frac{\partial T}{\partial Z}=-\frac{1}{Pr}\nabla^2 T \tag{5}$$

where the above equations are nondimensionalized by defining $X=x/H$, $Y=y/H$, $Z=z/H$,$P=p/\rho u_r^2$, $u_r=\nu/H$, $U=u/u_r$, $V=v/u_r$, $W=w/u_r$, $T=(t-t_c)/(t_h-t_c)$. P and T are non-dimensional pressure and temperature, respectively. U, V, and W are the non-dimensional velocity components in x-, y-, and z-directions, respectively. The other non-dimensional parameters in the above equations are Prandtl number $Pr=\nu/\alpha$, Rayleigh number $Ra=g\beta(t_h-t_c)H^3/\nu\alpha$ where β, ν, and α are the coefficient of volumetric expansion, kinematics viscosity, and thermal diffusivity, respectively. t_h is the temperature at the surface of the heated chip and t_c is the temperature of the top wall.

Boundary conditions for the velocity and temperature in non-dimensional form are as follows.

for $X=0$ and $X=A_x$, $U=V=W=0$, $\frac{\partial T}{\partial X}=0$ (for case 1), $T=0$ (for case 2)
for $Y=0$ and $Y=A_y$, $U=V=W=0$, $\frac{\partial T}{\partial Y}=0$ (for case 1), $T=0$ (for case 2)
for $Z=0$ and $Z=1$, $U=V=W=0$
for $Z=0$ $T=1$ (at chip), $\frac{\partial T}{\partial Z}=0$ (elsewhere)
for $Z=1$ $T=0$

The local heat transfer rate at the discretely heated chip is presented by means of local Nusselt number, which is obtained from

$$Nu=\left.\frac{-\partial T}{\partial Z}\right|_{z=0} \tag{6}$$

4. Method of solution

Eqs. (1)–(5) are discretized using staggered, nonuniform control volumes. In order to minimize the numerical diffusion errors, a third order accurate QUICK scheme [10] is used in approximating the advection terms. However, the QUICK scheme suffers from a lack of boundedness, i.e., it tends to give rise to non-physical oscillations in high gradient regions (numerical dispersion). Flux limiter is a remedy for such problems. Hence, a limiter, known as ULTRA-SHARP [11,12] is used. This high-order scheme proved to be superior to low-order schemes. To alleviate the convergence problems, the method is implemented in the solution procedure using the deferred correction approach suggested by Khosla and Rubin [13]. The SIMPLE algorithm [14] is used to couple momentum and continuity equations. The momentum equations are solved by applying one iteration of the strongly implicit procedure (SIP) of Stone [15], which is extended here to handle 3D problems. The discretization of the pressure correction equation results in a set of equations with a symmetric coefficient matrix which is solved by the conjugate gradient (CG) method [16] until the sum of absolute residuals has fallen by a factor of ten. On the other hand, the coefficient matrix of the set of equations resulting from the discretization of the energy equation is non-symmetric and solved iteratively by the Bi-CGSTAB method [17]. SSOR preconditioning [16] is used for accelerating the convergence rates of both the CG and the Bi-CGSTAB methods. In all calculations presented here, underrelaxation factors of 0.7, 0.7, 0.7, 0.7, and 0.8 were applied to U, V, W, P, and T, respectively.

The rate of convergence of the above solution method is high at the beginning of the calculation but it becomes worse after a few outer iterations. The reason is that the use of iterative solution procedure efficiently removes only those Fourier components of the error whose wavelengths are smaller than or comparable to the grid spacing. To avoid the excessively high computer times inherent in the solution of 3D natural convection problems, a full approximation storage (FAS) full multigrid (FMG) method [18] applied to 3D staggered grids is used to solve the problem which removes a wider spectrum of wavelengths efficiently. The equations are solved by a three level fixed V-cycle procedure starting at the coarsest grid and progressing to the finer grid level. For prolongation operations tri-linear interpolation is used for all variables. For restriction, the area weighted average procedure is used for all quantities defined on the control-volume surface such as velocities. The volume-weighted average procedure is adopted for all quantities defined at the control-volume center such as pressure and temperature.

In this work $66\times66\times42$ grids are used on the finest level with denser, uniform grid spacing on the chip and non-uniform grids elsewhere. The non-uniform grids have denser clustering near the chip and the wall boundaries. A finer grid of $102\times102\times62$ was also tested to check if varying in the grid spacing could increase the accuracy of the calculations. The results, which were obtained for $Ra=10^5$ indicate a maximum

Table 1
Comparison with the results of Ref. [19] ($A_x = 3.5$, $A_y = 2.1$, $A_z = 1.0$, $Pr = 2.5$, $Ra = 2 \times 10^4$)

	Ref. [19] $80 \times 80 \times 80$	Present $80 \times 80 \times 80$
Nu	2.57	2.576
U_{max}	17.20	17.199
$X(U_{max})$	2.41	2.380
$Y(U_{max})$	1.59	1.610
$Z(U_{max})$	0.81	0.814
V_{max}	3.27	3.256
$X(V_{max})$	1.77	1.784
$Y(V_{max})$	1.78	1.771
$Z(V_{max})$	0.21	0.217
W_{max}	20.78	20.550
$X(W_{max})$	1.77	1.716
$Y(W_{max})$	1.06	1.070
$Z(W_{max})$	0.52	0.510

relative difference of 1.2% in the vertical velocity profile. Additionally, the relative difference between both grids for the average Nusselt number on the chip is 1.1%.

To ensure convergence of the numerical algorithm the following criteria is applied to all dependent variables over the solution domain

$$\sum \left| \phi_{ijk}^{m} - \phi_{ijk}^{m-1} \right| \leq 10^{-3}$$

where ϕ represents a dependent variable U, V, W, P, and T; the indexes i, j, k indicate a grid point; and the index m the current iteration at the finest grid level.

The code was validated with the numerical results of Mukutmoni and Yang [19] for the bottom heated cavity with adiabatic side walls, having aspect ratios $A_x = 3.5$, $A_y = 2.1$, and $A_z = 1.0$, using a fluid with $Pr = 2.5$, at $Ra = 2 \times 10^4$. This corresponds to the case of a heated chip with $a_x = A_x$ and $a_y = A_y$. A comparison of the computations is given in Table 1, with the $80 \times 80 \times 80$ uniform grid results of Ref. [19]. It should be noted that the scaling, as well as the axes are different in the present investigation, so that appropriate conversions are used for comparison. It can be seen that the average Nusselt number differs by about 0.2% and the maximum vertical velocity by 1.1%

5. Results and discussions

Numerical simulations have been performed to elucidate the effect of Rayleigh number, chip lateral aspect ratio, and the sidewall boundary conditions on the natural convection cooling of a flush-mounted discrete heater on the bottom wall of a horizontal enclosure having aspect ratios of $A_x = 4$ and $A_y = 4$. The cooling fluid is air having a Prandtl number of 0.71. The range of Rayleigh numbers considered starts from 10^3 until the flow structure becomes unsteady where a steady converged solution could not be obtained. The lateral aspect ratios, a_y, of the considered chip are 1, 2 and 4 where the latter value corresponds to a heat source encompassing the whole enclosure width. First, adiabatic boundary conditions for the lateral walls are considered and then the effect of boundary conditions is investigated by assigning constant temperature to the four vertical sidewalls.

5.1. Flow and temperature fields: adiabatic sidewalls

The buoyancy-driven flow and temperature fields inside a horizontal cavity, with a discrete heat source of aspect ratios $a_x = 1$ and $a_y = 1$, flush-mounted with the bottom wall are illustrated by means of projection of flowlines and isotherms on mid x–z plane in Fig. 2(a)–(c) for Rayleigh numbers of 10^3, 10^5, and 10^6, respectively. The projection of flowlines on a particular plane is obtained from the in-plane components of the velocity vectors at that plane. For example, the projection of flowlines on mid x–z plane is obtained from the u and v components of the velocity vectors on that plane. The projection of flowlines on the mid x–z plane are not closed, but have a spiral form. The spiralling of the flowlines implies that the gradient of the out-of-plane velocity component ($\partial v/\partial y$) is non-zero indicating the existence of flow in y-direction. This can be observed from the flow patterns on the xy plane at $Z = 0.1$ (Fig. 3(a) and (b)), where the flowlines are no longer parallel to x-axis but diverge towards the lateral side walls.

For $Ra = 10^3$–10^5, the flow pattern is characterised by a single roll cell of nearly toroidal shape (Fig. 2(a) and (b)), with centers of rotation in the two sections of the toroid moving towards sidewalls as Ra increases. This basic flow structure has a vertical symmetry axis passing through the cavity center. The hot fluid rises in the central region as a result of buoyancy forces, until it reaches near the top wall where it turns radially outward, towards the sidewalls while it is cooled. Then it turns downward near those walls. Finally, the restriction imposed by the bottom wall forces the fluid to turn radially inward, receiving heat when it reaches the chip. The flow path is completed as the colder fluid is entrained to the ascending flow at the center of the cavity. At $Ra = 10^3$, as can be expected, heat transfer from the discrete heater is essentially dissipated via a conduction-dominated mechanism as indicated by the isotherm pattern shown in Fig. 2(a). For $Ra > 10^3$ the buoyant convection flow in the central region between the rolls distorts the isotherms field. The distortion of

the isotherm field increases with enhanced buoyancy as Ra increases, where the heat transfer becomes increasingly advection dominated. At the central region near the chip the buoyant flow distorts the isotherms and thus decreases the temperature gradients, with a resulting decrease of heat transfer rates at the central region of the chip, compared with the outer sections. With increase of Rayleigh number to 10^6 a transformation from a primarily toroidal roll pattern to a structure characterised by two small vortices near the sidewalls and an ascending flow in the region above the heater is indicated in Fig. 2(c). Furthermore, the thermal structure revealed by the isotherm plot in Fig. 2(c) clearly indicate the dominance of advection mechanism in cooling the discrete heater. No convergent steady flow solution could be obtained for $Ra = 10^7$. The velocity pattern on mid y–z plane exhibits the same counter rotating cell structure as that of mid x–z plane shown in Fig. 2(a)–(c) due to toroidal symmetry.

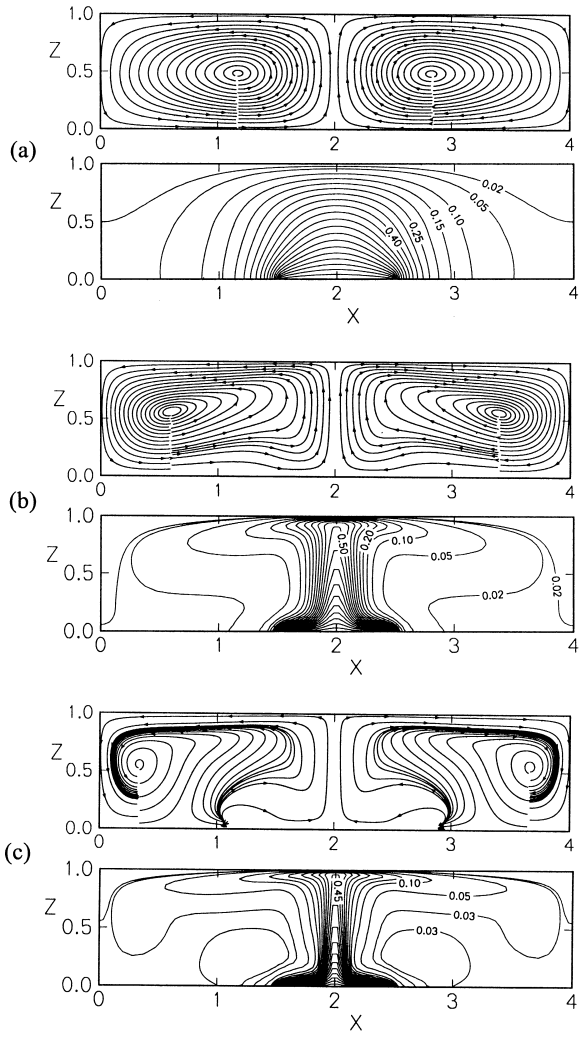

Fig. 2. Projection of flowlines (top) and isotherms (bottom) on mid vertical (x–z) plane for a discrete heater with $a_x = 1$ and $a_y = 1$, for (a) $Ra = 10^3$, (b) $Ra = 10^5$, and (c) $Ra = 10^6$.

The projection of flowlines on a horizontal plane near the bottom plate, at $z = 0.1L_z$, is illustrated in Fig. 3(a) and (b), for $Ra = 10^5$ and 10^6, respectively. The flow direction is radially inward from the sides of the cavity, which is the characteristic pattern at the bottom half of the toroidal roll cell for $Ra = 10^3$–10^5. At $Ra = 10^6$ the flow coming from the sidewalls is not able to reach the center (Fig. 3(b)) due to formation of vortices shown earlier in Fig. 2(c). Only the flow originating from the corner regions is able to reach the center.

The distribution of the W-velocity component of the induced flow at the x–y plane at $Z = 0.5$ is shown in Fig. 4(a)–(b) for $Ra = 10^3$ and 10^5. Although discrete heater is a square, at $Z = 0.5$ the induced buoyant jet diffuses into a circular form, the cross section of which contracts and magnitude increases with an increase in Rayleigh number. At $Ra = 10^5$ the descending flow is confined to a narrow section at the periphery of the cavity, resulting in higher downward velocities near the vertical walls.

To investigate the effect of the heater dimensions, the flow and temperature fields at $Ra = 10^5$ are reproduced in Fig. 5 for a heater of aspect ratios $a_x = 1$ and $a_y = 2$. For Rayleigh numbers 10^3 and 10^4 the toroidal roll cell structure is preserved and the flowline plots are similar to that shown in Fig. 2(a) and (b). However, this pattern is transformed to a different structure at $Ra = 10^5$, whereas for the square chip the flow structure consists of a toroidal roll at this Rayleigh number shown in Fig. 2(b).

The projection of flowlines on the horizontal plane at $z = 0.1L_z$ is shown in Fig. 6 for $Ra = 10^5$. The flow is characterized by almost a radially inward pattern for $Ra = 10^4$. At $Ra = 10^5$, the flowlines are bent along y-axis (Fig. 6), where the toroidal structure is lost, as shown earlier in Fig. 5. No steady-state solution could be obtained for $Ra = 10^6$ for the chip with aspect ratios $a_x = 1$ and $a_y = 2$.

The flow and temperature fields for a heater with aspect ratios $a_x = 1$ and $a_y = 4$, which stretches along the whole width of the bottom wall of the enclosure is shown in Fig. 7 for $Ra = 10^5$. The flow pattern consists of two counter rotating cells in the x–z plane for $Ra = 10^3$–10^5. No convergent steady state solution could be obtained for $Ra = 10^6$. The projection of flowlines on the horizontal plane at $z = 0.1L_z$ is shown in Fig. 8 for $Ra = 10^4$. The flow pattern is completely different than that of the previous cases studied where the chip aspect ratio, a_y, was less than 4. The flow is directed towards the centerline along x-direction near

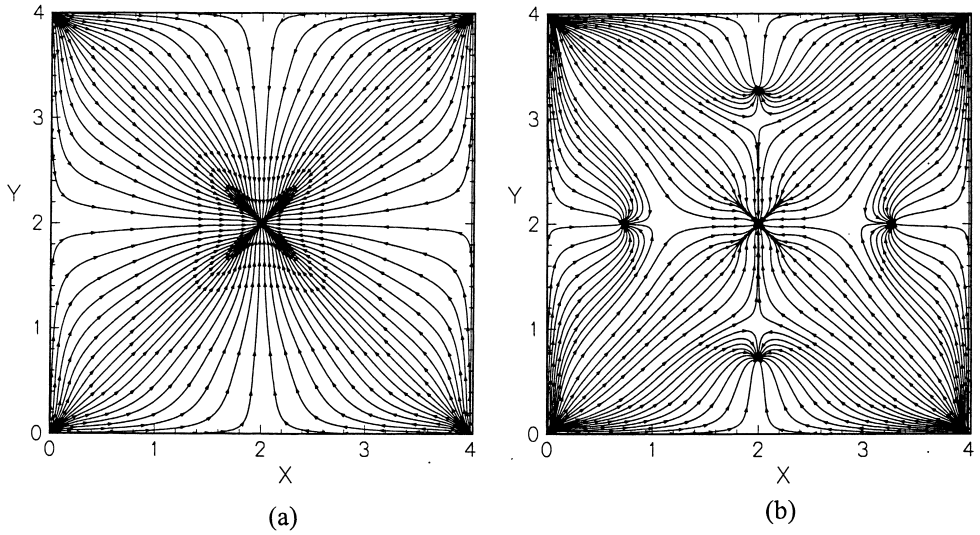

Fig. 3. Projection of flowlines on a horizontal plane at $z = 0.1L_z$ for a discrete heater with $a_x = 1$ and $a_y = 1$, for (a) $Ra = 10^5$ and (b) $Ra = 10^6$.

the bottom plate. This pattern prevails for all Rayleigh numbers studied between 10^3 and 10^5, for a chip with lateral aspect ratio $a_y = 4$. The carpet plot of the vertical component, W, of the velocity is depicted in Fig. 9 for a Rayleigh number of 10^5. The buoyant flow has two velocity peaks near the edges, which has not yet developed for lower Rayleigh numbers.

5.2. Heat transfer

In this section the attention is focused on the influence of the Rayleigh number on heat transfer from the discrete heater for different lateral aspect ratios, a_y, of the heater. Fig. 10 illustrates distribution of the local heat transfer rate along y-axis at $X = 2$ on the square

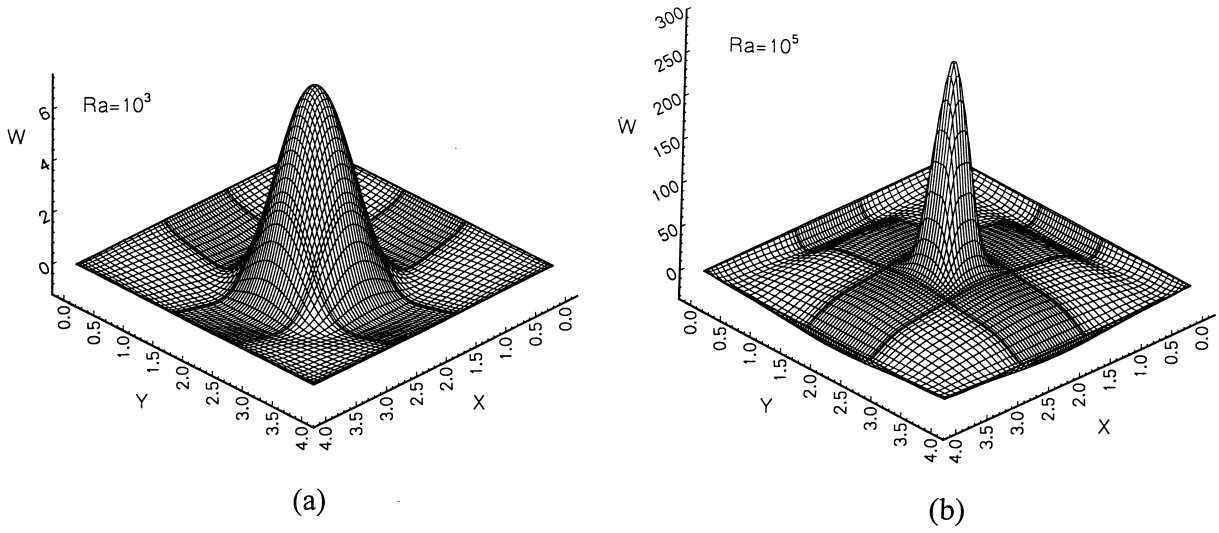

Fig. 4. Buoyant jet velocity in vertical direction, at $Z = 0.5$, for a discrete heater with $a_x = 1$ and $a_y = 1$, for (a) $Ra = 10^3$ and (b) $Ra = 10^5$.

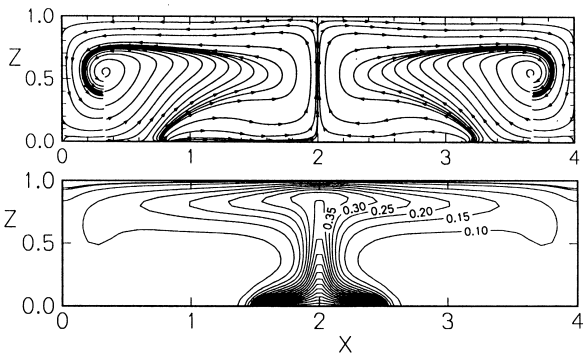

Fig. 5. Projection of flowlines (top) and isotherms (bottom) on mid vertical (x–z) plane for a discrete heater with $a_x = 1$ and $a_y = 2$, for $Ra = 10^5$.

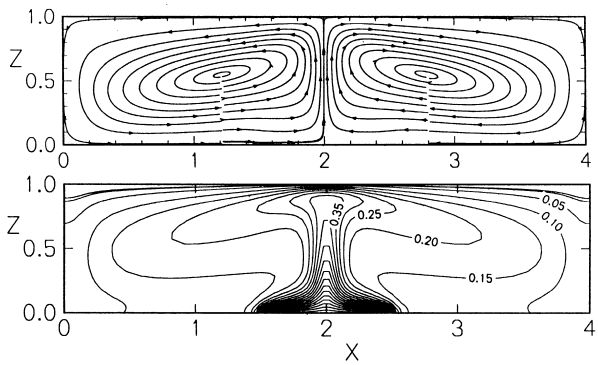

Fig. 7. Projection of flowlines (top) and isotherms (bottom) at mid vertical (x–z) plane for a discrete heater with $a_x = 1$ and $a_y = 4$, for $Ra = 10^5$.

heater with $a_x = 1$ and $a_y = 1$, for different Rayleigh numbers. In conformity with the toroidal roll cell structure illustrated in Figs. 2 and 3, the local Nusselt number features a corresponding variation attaining maximum values near the edges of the heater. This is a result of boundary layer development as the flow direction of the fluid over the heater surface is from the edges towards center. For $Ra = 10^3$ the local Nusselt number is close to 1 on the heater except the edges which indicates that the heat transfer mechanism is conduction dominated. For higher Rayleigh numbers, $Ra \geq 10^4$, the increasing influence of the buoyant convection leads to an increase in heat transfer on the heater surface except the center, which corresponds to a stagnation point.

Local heat transfer rate on a heater with aspect ratios $a_x = 1$ and $a_y = 2$ at $X = 2$ is displayed in Fig. 11 for $Ra = 10^3$–10^5. Again the Nusselt number is maximum near the edges of the heater due to boundary layer development on the heater induced by the counter rotating rolls.

For a strip heater stretching along the whole width of the enclosure with $a_x = 1$ and $a_y = 4$, the Nusselt number is close to unity for $Ra = 10^3$, which points out to a conduction dominated heat transfer mechanism over the heater surface (Fig. 12). The heat transfer is rather uniform over the heated surface for $Ra = 10^3$–10^4 but exhibits two maxima near the edges for $Ra = 10^5$ in conformity with the buoyant flow structure illustrated in Fig. 9. The rather uniform heat transfer rates along the whole width of the enclosure

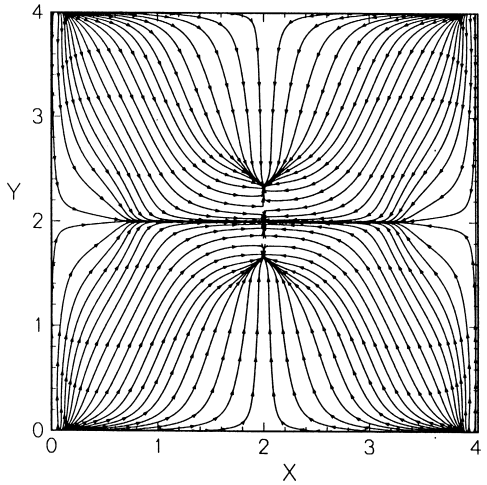

Fig. 6. Projection of flowlines on a horizontal plane on $z = 0.1L_z$ for a discrete heater with $a_x = 1$ and $a_y = 2$, for $Ra = 10^5$.

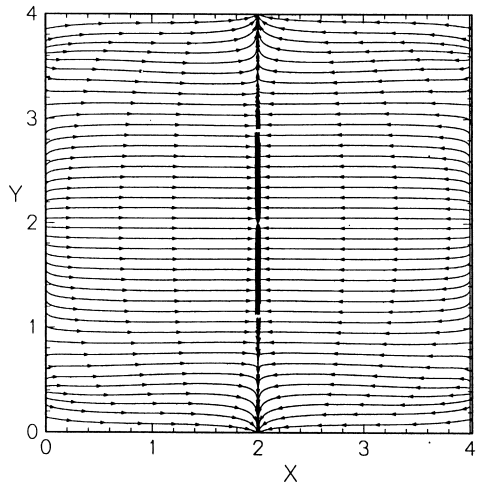

Fig. 8. Projection of flowlines on the horizontal plane at $z = 0.1L_z$ for a discrete heater with $a_x = 1$ and $a_y = 4$, for $Ra = 10^4$.

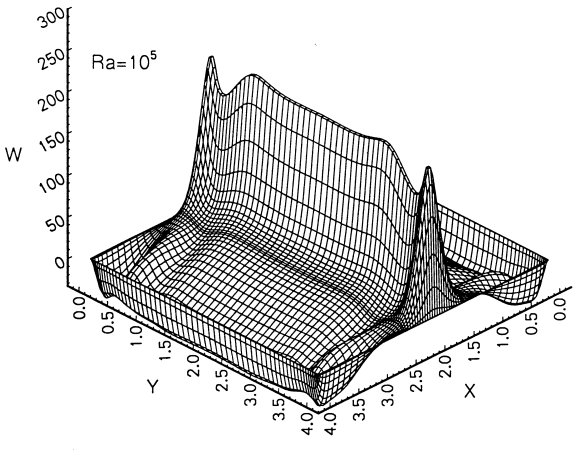

Fig. 9. Buoyant jet velocity in vertical direction, at $Z = 0.5$, for a discrete heater with $a_x = 1$ and $a_y = 4$, for $Ra = 10^5$.

bottom is in agreement with the experimental results of Polentini et al. [7]. However, studies on discrete heat sources mounted on the vertical surface of the enclosure show that heat transfer rates are non-uniform; heat transfer rate decreasing with the elevation of the heater on the wall. This suggests that a horizontal alignment of the heat sources should be preferred when uniform cooling is desired which is most often the case for electronic cooling. It can also be observed that the edge effects decrease as the length of the heater increases. Then, ample space should be provided between the electronic components to avoid forming a continuous heating surface so that edge effects can be maximized during cooling.

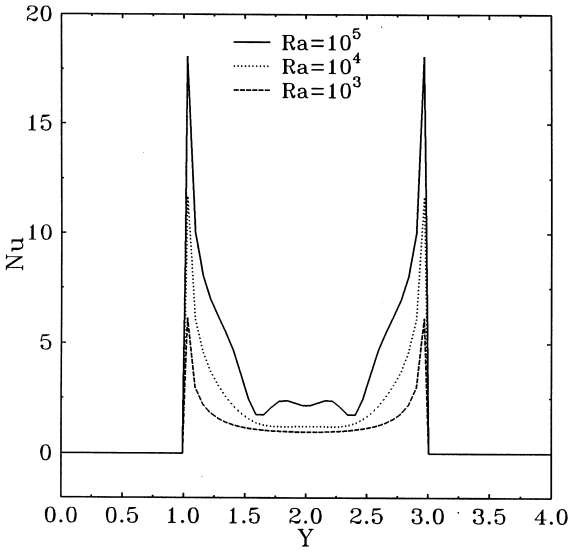

Fig. 11. Variation of Nusselt number on the discrete heater with $a_x = 1$ and $a_y = 2$.

5.3. Adiabatic vs. constant temperature sidewalls

When constant temperature sidewalls are considered instead of adiabatic sidewalls, the general flow pattern does not change. That is, the flow pattern always con-

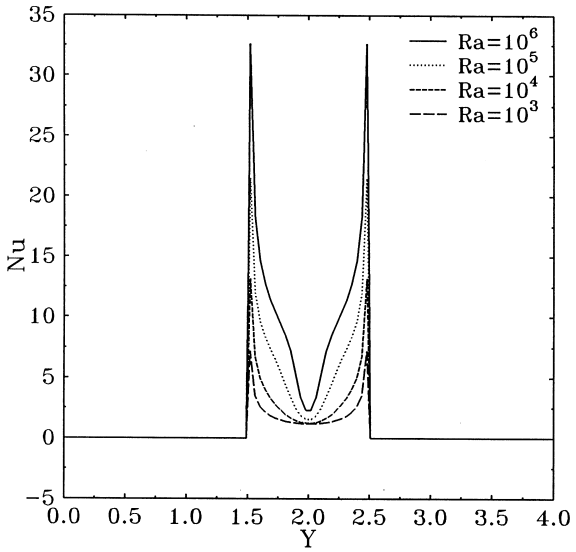

Fig. 10. Variation of Nusselt number on the discrete heater with $a_x = 1$ and $a_y = 1$.

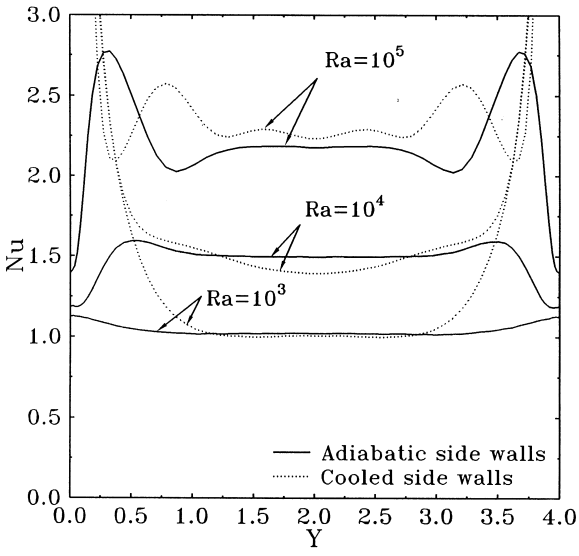

Fig. 12. Variation of Nusselt number on the discrete heater with $a_x = 1$ and $a_y = 4$.

sists of a toroidal roll. Hot fluid rises over the heater at the center of the cavity and cold fluid sinks near the sidewalls. Therefore the constant temperature sidewall roll pattern is closely similar to the adiabatic sidewall case. For a square heater ($a_x = 1, a_y = 1$) and rectangular heater ($a_x = 1, a_y = 2$) the Nusselt number distribution curves are almost coincident with the adiabatic wall case. On the other hand, when the heater stretches over the entire width of the cavity the Nusselt number increases considerably near the cavity walls. This is a result of the discontinuity formed at the corner where the hot temperature heater is in contact with the cold temperature vertical walls. Even higher Nu values are predicted as the mesh size is further refined. In fact, the analytical solution would give infinite Nusselt numbers at the edges. However, such a situation is impossible to arrange experimentally where a gradual change of temperature would be experienced both in the heater and the cold walls near the corner, resulting in finite Nusselt number there.

6. Concluding remarks

A detailed numerical analysis of horizontal discrete heaters of different length/width ratios, flush-mounted with the bottom wall of a cavity has been performed. The aspect ratios of the enclosure were kept constant at $A_x = 4$ and $A_y = 4$. The flow pattern, consists of a toroidal roll cell in the cavity for a square heater with aspect ratios, $a_x = 1$ and $a_y = 1$, for $Ra = 10^3$–10^5. The toroidal roll cell structure is destroyed at a Rayleigh number between 10^5 and 10^6 and a completely different flow pattern is formed having two vortices near the top corners of the cavity. Although the heater cross section is square, the buoyant jet diffuses into a circular form above the bottom plate. For a rectangular heater with $a_x = 1$ and $a_y = 2$ the transition from toroidal roll cell structure takes place between Rayleigh numbers 10^4 and 10^5. For a heater stretching over the entire width of the bottom plate ($a_x = 1, a_y = 4$), a two roll cells pattern exists, with axes of rotation parallel to the longer dimension of the chip, for all Rayleigh numbers studied between 10^3 and 10^5. A "saddle backed" spanwise profile of the buoyant jet velocity is formed with two off-center peaks, for a heater with $a_x = 1, a_y = 4$.

The toroidal roll cell structure induces a boundary layer development at the edges of the discrete heater as the flow direction of the fluid over the heater surface is from the edges towards the center. As a result, the heat transfer is maximum at the edges of the discrete heater and minimum at the center. The edge effects decrease as the length of the heater increases. For the strip heater stretching along the whole width of the cavity the heat transfer is rather uniform, which is a highly desirable feature when cooling electronic components, suggesting that a horizontal rather than a vertical arrangement of a line of such devices is preferable.

References

[1] M. Keyhani, V. Prasad, R. Cox, An experimental study of natural convection in a vertical cavity with discrete heat source, J. Heat Transfer 110 (1988) 616–624.
[2] M.L. Chadwick, B.W. Webb, H.S. Heaton, Natural convection from two-dimensional discrete heat sources in a rectangular enclosure, Int. J. Heat Mass Transfer 34 (1991) 1679–1693.
[3] C.J. Ho, J.Y. Chang, A study of natural convection heat transfer in a vertical rectangular enclosure with two-dimensional discrete heating: effect of aspect ratio, Int. J. Heat Mass Transfer 37 (1994) 917–925.
[4] Y. Ju, Z. Chen, Numerical simulation of natural convection in an enclosure with discrete prodruding heaters, Numerical Heat Transfer, Part A 30 (1996) 207–218.
[5] T.J. Heindel, F.P. Incropera, S. Ramadyani, Enhancement of natural convection heat transfer from an array of discrete heat sources, Int. J. Heat Mass Transfer 39 (1996) 479–490.
[6] H.Y. Wang, F. Penot, J.B. Sauliner, Numerical study of a buoyancy-induced flow along a vertical plate with discretely heated integrated circuit packages, Int. J. Heat Mass Transfer 40 (1997) 1509–1520.
[7] M.S. Polentini, S. Ramadhyani, F.P. Incropera, Single phase thermosyphon cooling of an array of discrete heat sources in a rectangular cavity, Int. J. Heat Mass Transfer 36 (1993) 3983–3996.
[8] R.J. Goldstein, R.J. Volino, Onset and development of natural convection above a suddenly heated horizontal surface, J. Heat Transfer 117 (1995) 808–821.
[9] J. Pallares, I. Cuesta, F.X. Gran, F. Giralt, Natural convection in a cubical cavity heated from below at low Rayleigh numbers, Int. J. Heat Mass Transfer 39 (1995) 3233–3247.
[10] B.P. Leonard, A stable and accurate convective modelling procedure based on quadratic upstream interpolation, Comput. Methods Appl. Mech. Engng 19 (1979) 59–98.
[11] B.P. Leonard, S. Mokhtari, Beyond first order upwinding: the ULTRA-SHARP alternative for nonoscillatory steady-state simulation of convection, Int. J. Numer. Methods Eng 30 (1990) 729–766.
[12] B.P. Leonard, J.E. Drummond, Why you should not use 'Hybrid', 'Power Law' or related exponential schemes for convective modelling: there are much better alternatives, Int. J. Numer. Meth. Fluids 20 (1995) 421–442.
[13] P.K. Khosla, S.G. Rubin, A diagonally dominant second-order accurate implicit scheme, Comput. Fluids 2 (1974) 207–209.
[14] S.V. Patankar, Numerical Heat Transfer and Fluid Flow, McGraw-Hill, New York, 1980.
[15] H.L. Stone, Iterative solution of implicit approximations

of multi-dimensional partial differential equations, SIAM J. Numer. Analysis 5 (1968) 530–558.
[16] W. Hackbush, Iterative Solution of Large Sparse System of Equations, Springer-Verlag, New York, 1994.
[17] H.A. Van der Vorst, BiCGSTAB: a fast and smoothly converging variant of Bi-CG for the solution of non-symmetric linear systems, SIAM J. Sci. Statist. Comput 13 (1992) 631–644.
[18] M. Hortmann, M. Peric, G. Scheuerer, Finite volume multigrid prediction of laminar natural convection: bench-mark solutions, Int. J. Numer. Methods in Fluids 11 (1990) 189–207.
[19] D. Mukutmoni, K.T. Yang, Rayleigh-Benard convection in a small aspect ratio enclosure. Part I: bifurcation to oscillatory convection, J. Heat Transfer 115 (1993) 360–366.